Solidlike to liquidlike behavior of Cu diffusion in superionic Cu_2X (X = S, Se): An inelastic neutron scattering and *ab initio* molecular dynamics investigation

Sajan Kumar,[1,2] M. K. Gupta,[1,2,*] Prabhatasree Goel,[1] R. Mittal,[1,2,†] Olivier Delaire,[3] A. Thamizhavel,[4] S. Rols,[5] and S. L. Chaplot[1,2]

[1]*Solid State Physics Division, Bhabha Atomic Research Centre, Trombay, Mumbai 400085, India*
[2]*Homi Bhabha National Institute, Anushaktinagar, Mumbai 400094, India*
[3]*Department of Mechanical Engineering and Materials Science, Duke University, North Carolina 27708, USA*
[4]*Tata Institute of Fundamental Research, Homi Bhabha Road, Colaba, Mumbai 400005, India*
[5]*Institut Laue-Langevin, Boîte Postale 156, 38042 Grenoble Cedex 9, France*

(Received 3 January 2022; accepted 4 May 2022; published 26 May 2022)

Cu_2Se and Cu_2S are excellent model systems of superionic conductors with large diffusion coefficients that have been reported to exhibit different solidlike and liquidlike Cu-ion diffusion. In this paper, we clarify the atomic dynamics of these compounds with temperature-dependent *ab initio* molecular dynamics (AIMD) simulations and inelastic neutron scattering experiments. Using the dynamical structure factor and Van Hove correlation function, we interrogate the jump time, hopping length distribution, and associated diffusion coefficients. In cubic Cu_2Se at 500 K, we find solidlike diffusion with Cu jump lengths matching well the first-neighbor Cu-Cu distance of ∼3 Å in the crystal, and clearly defined optic phonons involving Cu vibrations. Above 700 K, the jump-length distribution becomes a broad maximum centered around 4 Å, spanning the first and second neighbor lattice distances, and a concurrent broadening of the Cu-phonon density of states. Further, above 900 K, the Cu diffusion becomes close to liquidlike, with distributions of Cu atoms continuously connecting crystal sites, while the vibrational modes involving Cu motions are highly damped, though still not fully overdamped as in a liquid. At low temperatures, the solidlike diffusion is consistent with previous x-ray diffraction and quasielastic neutron scattering experiments, while the higher-temperature observation of the liquidlike diffusion is in agreement with previous AIMD simulations. We also report AIMD simulations in Cu_2S in the hexagonal and cubic superionic phases, and observe nearly liquidlike diffusion above ∼500 K. The calculated ionic conductivity is in fair agreement with reported experimental values.

DOI: 10.1103/PhysRevMaterials.6.055403

I. INTRODUCTION

In recent years, the world has seen an increased demand for green energy, which has the potential to mitigate the threat of global warming. Superionic materials play an important role in the domain of energy conversion and storage [1–7]. Copper chalcogenides (Cu_2X, X = Se, S) are superionic compounds with excellent thermoelectric properties [8,9], attributed in part to the melting behavior of the Cu sublattice in Cu_2X (X = S, Se) at elevated temperatures, which results in an intrinsically low thermal conductivity [10–12]. Besides their potential as being thermoelectric, these compounds are candidates for photovoltaics and photoelectrodes owing to their favorable electrical and optical properties [8,13–17]. These materials show a rich phase diagram with temperature and also with Cu off-stoichiometry [18,19], including high-temperature cubic phases that exhibit fast Cu-ion diffusion [20,21]. The added advantages of these compounds are that they are cheap, safer, abundant, and nontoxic, but the limitation is that high temperature is required for operation [22]. Typically, these two properties are required for a compound to exhibit superionicity: availability of a large number of vacant sites and low activation energy, so that ions can easily hop between available sites.

Copper selenide, Cu_2Se, crystallizes in a monoclinic phase (space group $C2/c$, α phase) at ambient conditions, while above 414 K, it transforms to a superionic cubic phase (space group $Fm\text{-}3m$, β phase) [22–24]. The β phase of Cu_2Se shows an ordered structure and exhibits low ionic conductivity [23]. In the high-temperature α phase, the Cu diffusion coefficient is $\sim 10^{-4}$–10^{-5} $cm^2\ s^{-1}$ at 670 K and the corresponding ionic conductivity is 1–2 $\Omega^{-1}\ cm^{-1}$, which is three orders of magnitude higher than the α phase at room temperature and similar to molten salts [25,26]. The superionic phase can be stabilized to ambient temperature in Cu-deficient $Cu_{2-x}Se$ [27]. In the superionic β phase at 415 K, the Se atoms occupy the 4a Wyckoff sites (fcc position in cubic phase), and Cu atoms partially occupy the 4b (octahedral), 8c (tetrahedral), and 32f Wyckoff sites (encloses the 8c tetrahedral sites) with fractional occupancies ∼0.001, ∼0.72, and ∼0.07, respectively [Fig. 1(a)]. The 32f sites form a tetrahedral cage around the 8c site [28–30].

The sister compound Cu_2S crystallizes in an orthorhombic phase ($Pna2_1$) at temperatures below 202 K, and exhibits

*mayankg@barc.gov.in
†rmittal@barc.gov.in

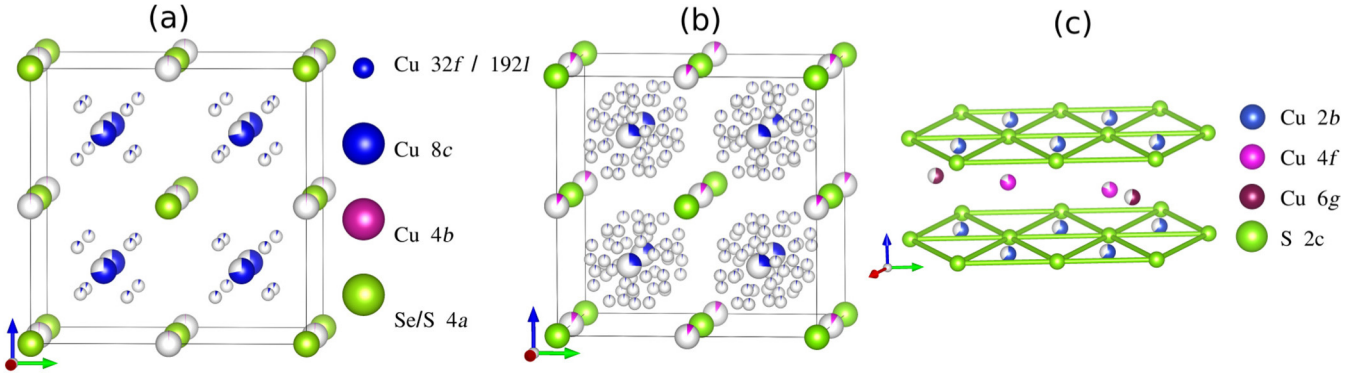

FIG. 1. The crystal structure of (a) Cu_2Se and (b) Cu_2S in the high-temperature cubic phase (Fm-3m). The Cu occupancies are (a) Cu_2Se-8c (0.72), 4b (0.0), 32f (0.07); and (b) Cu_2S- 8c (0.26), 4b (0.09), 192l (0.03). The Cu occupancies are shown by partially colored large and small spheres, while fully occupied S/Se are shown by green spheres (see legends). (c) The crystal structure of superionic hexagonal phase of Cu_2S. Cu partially occupies 2b, 4f, and 6g Wyckoff sites, while S fully occupies the 2c Wyckoff site.

many polymorphs above this temperature: tetragonal ($P4_32_12$) above 202 K, hexagonal ($P6_3/mmc$, β phase) above 380 K, and cubic phases (Fm-3m, γ phase) above 700 K [31–36]. The hexagonal and cubic phases of Cu_2S show superionic behavior [37]. In the hexagonal β phase, the S atoms occupy the 2c Wyckoff sites, while the Cu atoms partially occupy the 6g, 4f, and 2b Wyckoff sites with fractional occupancies of ∼0.19, ∼0.41, and ∼0.62, respectively [Fig. 1(c)] [31,35]. In the superionic cubic γ phase, the S atoms occupy the 4a Wyckoff sites and Cu atoms partially occupy the 4b, 8c, and 192l Wyckoff sites with fractional occupancies ∼0.09, ∼0.26, and ∼0.03, respectively [Fig. 1(b)] [35]. The 192l sites form a cage around the 8c site. The details about the various structural phase transitions and range of stability of Cu_2X (X = S, Se) are summarized in Table SI in the Supplemental Material [38].

Superionic materials are often described as hybrid solid-liquid structures [8,37,39–41], with the notion that at least one sublattice has melted and shows significant diffusion. However, the molten sublattice is usually not a simple liquid. For example, in the case of superionic Li_2O, Li occupies 8c tetrahedral sites, and undergoes [42,43] jump diffusion from one lattice site to another, but with the jump time remaining much smaller than the residence time at either lattice site. Therefore, the time-averaged structure shows a high probability of the occurrence of the Li atoms at the sublattice sites, and therefore the crystal structure and its sites remain well defined in this case. As we shall discuss below, the diffusion of Cu in Cu_2X is more complex, in part because the Cu atoms can reside at many available sites in the crystal, as noted above.

Many investigations of Cu diffusion in Cu_2Se using quasielastic neutron scattering (QENS) have been reported [21,23,44]. These QENS results have generally been analyzed on the basis of jump-diffusion models assuming atomic jumps between fixed atomic sites in the crystal. However, the reported time and length scales of atomic jumps do not agree well with each other among these prior works. *Ab initio* molecular dynamics (AIMD) simulations on cubic Cu_2Se in Ref. [44] indicated a jump-diffusion behavior between the different tetrahedral (8c) and octahedral sites (4b) in the crystal. In contrast, another recent AIMD study [20] on cubic Cu_2S and Cu_2Se proposed a liquidlike diffusion mechanism, with short residence times for Cu ions at the crystallographic sites. The AIMD studies [36,37] on hexagonal Cu_2S reported liquidlike anisotropic Cu diffusion at 450 K.

In the present study, we resolve the ambiguity in the nature of diffusion in earlier works [20,21,23,36,37,44], i.e., whether it is solidlike jump diffusion between sublattice sites, or a liquidlike diffusion with very short residence times and low occupation probabilities of the Cu sublattice crystallographic sites, by performing extensive AIMD simulations as a function of temperature. We have identified, using the Van Hove position-time correlation function, that the differences arose due to the use of different temperatures in previous works. Specifically, we find that that the nature of diffusion is jumplike between crystal lattice sites at low temperature. The Chudley-Elliott (CE) jump-diffusion model is applicable in these cases. At high temperatures, the diffusion is found to change to a liquidlike behavior, which is not jumplike between the crystal sites. In the case of the liquidlike diffusion, the CE jump-diffusion model is not applicable. In some of the literature [20,21,36,37], the jumplike diffusion is also termed liquidlike when the magnitude of the diffusion coefficient is close to that typically in a liquid, irrespective of the nature of the diffusion process. These results have important implications for the understanding of ionic conductivity, as well as the thermal conductivity in these materials. We also report inelastic neutron scattering measurements of the phonon spectra in Cu_2Se as a function of temperature, which sheds some light on the nature of diffusion and the possible relationship of phonons and diffusion.

II. EXPERIMENTAL DETAILS

We have prepared the Cu_2Se samples using the solid-state reaction method and characterized them using x-ray diffraction at room temperature. All the peaks were well indexed with space group Fm-3m (Fig. S1 in the Supplemental Material [38]). The refined Cu occupancies showed that the sample is slightly Cu deficient, with an estimated composition of $Cu_{1.85}Se$. We used 10 g of a polycrystalline sample of $Cu_{1.85}Se$ to measure the phonon density of states (PDOS) in the temperature range from 100 to 450 K. The

measurements were carried out using the time-of-flight IN4C spectrometer at the Institut Laue Langevin (ILL), France. The spectrometer detector bank covers a wide range of scattering angles (10°–110°). The measurements were conducted with 14.2 meV incident neutron energy in the energy gain mode. The neutron-weighted phonon density of states, $g^{(n)}(E)$, was obtained from the measured dynamic structure factor $S(Q, E)$ as given by [45–47]

$$g^{(n)}(E) = A\left\langle \frac{e^{2W(Q)}}{Q^2} \frac{E}{n(E,T) + \frac{1}{2} \pm \frac{1}{2}} S(Q,E) \right\rangle, \quad (1)$$

where A is a normalization constant and Q, $2W$, and E are the momentum transfer, Debye-Waller factor, and phonon energy. $n(E,T)$ is the Bose-Einstein population factor for phonon energy E at temperature T. The $\pm$ sign corresponds to energy loss/gain of the neutron. The total neutron-weighted density of states, $g^{(n)}(E)$, is related to the atomic partial density of states $g_k(E)$ as follows:

$$g^n(E) = B \sum_k \left(\frac{4\pi b_k^2}{m_k} \right) g_k(E). \quad (2)$$

Here B, b_k, and m_k are the normalization factor, the neutron scattering length, and the mass of the kth atom.

III. COMPUTATIONAL DETAILS

We used density functional theory (DFT) for lattice and molecular dynamics simulations as implemented within the software package VASP (Vienna *ab initio* software package) [48,49]. The simulations were performed in the generalized gradient approximation (GGA) with the Perdew-Burke-Ernzerhof (PBE) exchange-correlation functional and projected augmented wave (PAW) pseudopotentials with a kinetic energy plane-wave cutoff of 900 eV [50,51].

The lattice dynamics calculations of Cu_2Se and Cu_2S were performed only in the ordered phase (i.e., monoclinic phase in Cu_2Se, orthorhombic and tetragonal phase in Cu_2S). For phonon calculations, we took the optimized structure and displaced symmetrically inequivalent atoms by 0.03 Å in the $\pm x$, $\pm y$, and $\pm z$ directions and calculated the forces using Hellmann-Feynman theorem, which the PHONOPY software [52] then used to compute the phonon dynamical matrix and dispersions. A $2 \times 2 \times 1$ k-point mesh in the monoclinic Cu_2Se, and a $2 \times 2 \times 2k$-point mesh in orthorhombic and tetragonal Cu_2S were used. The k points were generated using the Monkhorst-Pack method [53]. The force convergence criterion was set to 10^{-3} eV/Å^2, and the energy convergence criterion was set to 10^{-8} eV.

The *ab initio* molecular dynamics simulations (AIMD) simulations were performed in an NVT ensemble using the Nosé-Hoover thermostat. The simulation was run for 60 ps with 2 fs time steps. We equilibrated the system for ∼10 ps to attain the desired temperature. Simulations were executed for different phases with different temperatures (for Cu_2Se β phase 500–900 K, α phase 100–300 K, and for Cu_2S γ phase 750–1100 K, β phase 300–700 K, orthorhombic 100 K, tetragonal 300 K). The supercell dimensions used in AIMD simulations in different phases of Cu_2S and Cu_2Se phases are given in Table SII in the Supplemental Material [38]. A single k-point sampling of the Brillouin zone at the zone center and an energy convergence of 10^{-6} eV were chosen.

The phonon density of states (PDOS) $g(E)$ was calculated from AIMD simulations by taking the Fourier transform of the velocity autocorrelation function [54].

$$g(E) = \sum_{i=1}^{N} \frac{\int \boldsymbol{v}_i(0) \cdot \boldsymbol{v}_i(t) e^{iEt/\hbar} dt}{\langle \boldsymbol{v}_i(0) \cdot \boldsymbol{v}_i(0) \rangle}, \quad (3)$$

where v_i(t) is the ith atom velocity at time t and N is the total number of atoms in the supercell. The raw PDOS data have been smoothened using a Gaussian resolution function with FWHM of 1 meV.

The diffusion coefficient D has been estimated from three different techniques, namely, by using the mean-squared displacement (MSD), the velocity autocorrelation (VACF), and the dynamical structure factor $S(Q, E)$. We have calculated the time dependence of MSD using the following relationship [55,56],

$$\langle u^2(\tau) \rangle = \frac{1}{N_{\text{ion}}(N_{\text{step}} - N_\tau)} \sum_{i=1}^{N_{\text{ion}}} \sum_{j=1}^{N_{\text{step}} - N_\tau} |\boldsymbol{r}_i(t_j + \tau) - \boldsymbol{r}_i(t_j)|^2, \quad (4)$$

where $\boldsymbol{r}_i(t_j)$ is the ith atom position at the jth time step, $N_\tau = \tau/\delta$, δ being the time step in the simulatio; N_{step} is the total number of simulation steps; and N_{ion} is the total number of a given element (Cu, S, Se) in a supercell. Using this time dependence, we estimated the diffusivity D as given by [57]

$$\langle D(T) \rangle = \langle u^2(\tau) \rangle / 6\tau. \quad (5)$$

In addition, we also calculated D by integrating the velocity autocorrelation function (VACF) as given by

$$D = \int \boldsymbol{v}_i(0) \cdot \boldsymbol{v}_i(\tau) d\tau. \quad (6)$$

A few experimental and simulation investigations have discussed the Cu diffusion behavior in the superionic phase of Cu_2Se; however, the values of D estimated from different techniques (QENS, impedance spectroscopy, and simulations) shows significant variance (10^{-5}–10^{-7} cm^2 s^{-1}) [20,21,23,44]. Hence, we performed a detailed investigation of Cu diffusion using several approaches. Further, to address the ambiguity from QENS measurements, we have calculated the dynamical structure factor, $S(Q, E)$, using long AIMD trajectories of ∼150 ps.

Usually, the stochastic dynamics is analyzed by fitting the $S(Q, E)$ measured by QENS with one Lorentzian function and one delta function convoluted with the resolution function of the instrument. The Q dependence of the half width at half maximum (HWHM) of the Lorentzian function provides information about the diffusion characteristics [58]. For localized diffusion, HWHM usually does not show significant variation with Q, while for long-range diffusion, HWHM in the low Q regime is characterized by a Q^2 dependence. Further, in the case of solid-state diffusion, the Q-dependent HWHM data may be fitted using jump-diffusion models, such as the Chudley-Elliott (CE) mode [58–60] to get the mean jump length and average residence time at a site. The CE model assumes a fixed jump length, and the Q-dependent

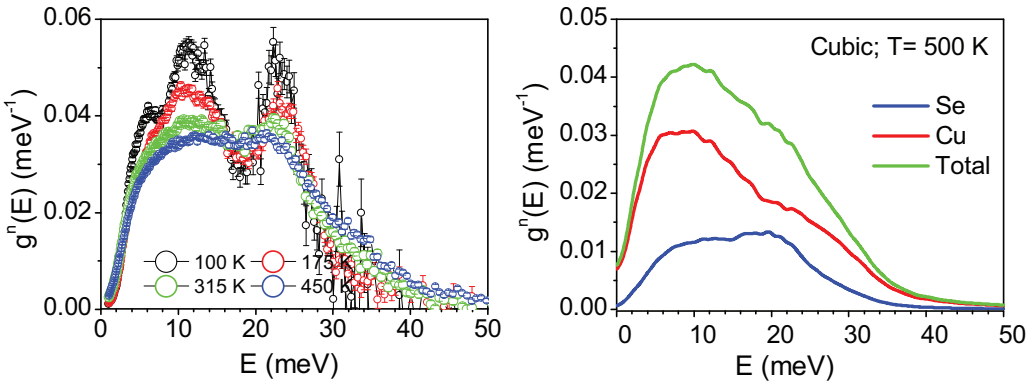

FIG. 2. (a) Temperature dependence of neutron-weighted PDOS, $g^{(n)}(E)$, of cubic $Cu_{1.95}Se$ from INS measurements. (b) AIMD calculated partial contributions of Cu and Se to $g^{(n)}(E)$ and the total at 500 K.

HWHM is given by

$$\Gamma(Q) = \frac{\hbar}{\tau}\left(1 - \frac{\sin(Qd)}{(Qd)}\right), \tag{7}$$

where τ is the mean residence time, and d is the jump length, and the diffusion constant D is given by

$$D = d^2/6\tau. \tag{8}$$

The self–Van Hove correlation function $g_s(r,t)$ shows the probability of finding an atom at distance r at the time t, with initial space and time coordinates of $(r = 0, t = 0)$. The singularities or peaks in the self–Van Hove correlations indicate the presence of jump diffusion through well-defined sites. The self–Van Hove correlation functions $g_s(r,t)$ are defined as [54,61]

$$g_s(r,t) = \frac{1}{N}\left\langle \sum_{i=1}^{N} [r - |\vec{r_i}(t) - \vec{r_i}(0)|] \right\rangle$$

N is the number of particles; $\vec{r}_i(t)$ is the position of the ith atom at time t .

IV. RESULTS AND DISCUSSIONS

A. Temperature dependence of phonon spectra using INS and AIMD simulations

The temperature-dependent PDOS of $Cu_{1.95}Se$ was measured from 100 to 450 K [Fig. 2(a)]. This temperature range covers the monoclinic to cubic phase transition at 414 K. The energy range of the phonon spectrum extends up to 40 meV. We observe that at 100 K, the INS spectra show sharp and well-defined peaks at 8, 12, and 22 meV as shown in Fig. 2(a). Our INS results are in good agreement with those of Voneshen *et al.* [21], although the energy resolution of the present data is superior due to the use of a smaller incident neutron energy and use of the neutron energy gain mode. Further, we have also calculated the partial contributions of Cu and Se to the PDOS and found that both atoms contribute to the entire spectral range of vibrations [Fig. 2(b)]. We note that the phonon dispersion relation of the acoustic phonons has been measured [30] in $Cu_{1.85}Se$ up to ∼15 meV, which appears to be consistent with the present PDOS measurements. We have also performed lattice dynamics calculation in the monoclinic phase of Cu_2Se and low-T phases (tetragonal and orthorhombic phases) at $T = 0$ K (Fig. S2 in the Supplemental Material [38]). We found that the phonon spectra in the ordered low-T phases show sharp peaks in the PDOS.

At high temperatures, the peaks in the measured phonon spectrum get significantly broadened [Fig. 2(a)]. The considerable broadening is attributed to large anharmonic lattice vibrations and Cu diffusion. To account for the anharmonic effects on the phonon spectrum, we performed AIMD calculations in the superionic cubic phase of Cu_2X (X = S, Se). In Fig. 3, we show the total PDOS of Cu_2X (X = S, Se) computed from AIMD in the superionic cubic phase at elevated temperatures. The PDOS does not show any sharp peak, and at elevated temperatures, the PDOS tends to a finite value at zero energy for both compounds, which is a signature of diffusion. Further, the PDOS value at $E = 0$ increases with temperature, which also indicates a faster diffusion at higher temperatures. We also calculated the partial PDOS of different phases of Cu_2X (X = S, Se) to see the contribution from different species to the PDOS and found that the finite PDOS at zero energy is mainly contributed from Cu dynamics (Figs. S2 and S3 in the Supplemental Material [38]). This further confirms that Cu is the only mobile ion at elevated temperatures, while S/Se atoms form a more rigid crystalline framework. Further, the phonon spectral weight shifts towards lower energies upon warming in both compounds, which can be attributed to damping of strongly anharmonic phonon modes in the superionic regime. However, it is important to note that the phonon spectrum of the Cu atoms persists up to high energies in the superionic phase indicating that a fast vibrational behavior of the Cu atoms remains despite the fast diffusion. This suggests that the nature of the diffusion continues to be jumplike up to moderate temperatures of ∼700 K, with the atoms spending significant time undergoing vibrations around rest positions between jumps, as is characteristic in a solid. At higher temperatures ∼900 K, the diffusion becomes closer to liquidlike. Therefore, we will discuss in the next section how the diffusion process is rather complex, involving both localized diffusion and long-range diffusion.

Besides the superionic cubic phase, we also computed the PDOS of Cu_2S in the hexagonal superionic phase, which exists between 370 and 700 K (Fig. S3 in the Supplemental Material [38]). Here also, a finite value of PDOS at $E = 0$

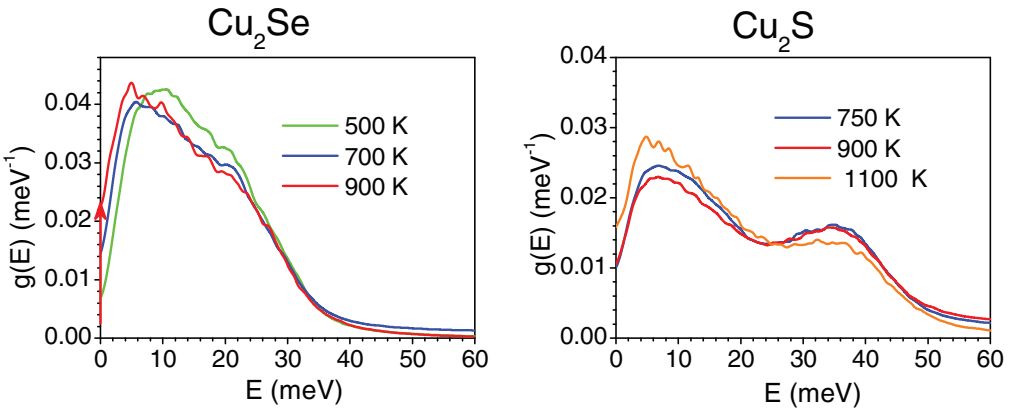

FIG. 3. The AIMD calculated temperature-dependent total PDOS, $g(E)$ in superionic-cubic phase of (a) Cu_2Se and (b) Cu_2S. The presence of nonzero PDOS at zero energy corresponds to Cu diffusion.

infers the presence of Cu diffusion; however, it is relatively less in magnitude than that in the superionic cubic phase.

B. Cu diffusion in Cu_2X (X = S, Se) and Van Hove correlations $g_s(r, t)$

In Fig. 4, we show the calculated MSD of Cu in Cu_2S and Cu_2Se at different temperatures. The Cu MSD shows a nearly linear increase with time, characteristic of diffusion. However, the MSD values for Se/S oscillate about mean values consistent with a solid framework structure (Fig. S4 in the Supplemental Material [38]). To investigate the Cu-Cu and Cu-S/Se distances in the superionic cubic phase, we also calculated the time-averaged pair distribution function (PDF) from AIMD trajectories in superionic phases of Cu_2X (X = S, Se) (Fig. S5 in the Supplemental Material [38]). In both compounds, the first-neighbor peak for the Cu-Cu and Cu-Se PDF is quite sharp, while the peaks corresponding to farther neighbors are much broader and more difficult to resolve.

In the superionic hexagonal phase of Cu_2S, interestingly, we find that slightly different c/a lattice-constant ratios in the MD simulation could lead to nearly isotropic or anisotropic diffusion. The work by Wang *et al.* [36] used the experimental structure by Will *et al.* ($c/a = 1.67$) [35] leading to anisotropic diffusion. We have also performed additional AIMD at 450 K using the same experimental structure and found similar anisotropic Cu diffusion behavior as reported by Wang *et al.* [36]. However, our AIMD simulation using a different experimental structure reported by Buerger and Wuensch ($c/a = 1.77$) [31] leads to nearly isotropic diffusion. However, at a low temperature of 300 K, we find

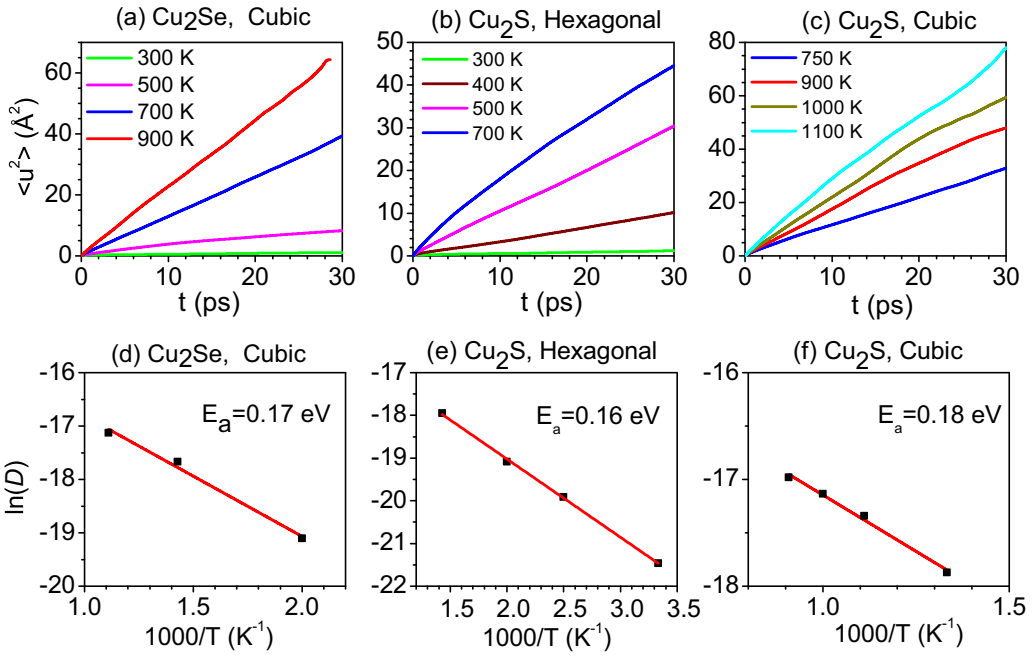

FIG. 4. (a)–(c) The calculated MSD of Cu atoms in Cu_2Se and Cu_2S at different temperatures using AIMD simulations performed in superionic phases. (d)–(f) Calculated temperature dependence of diffusion coefficient (D) estimated from MSD slope and estimated activation barrier E_a for Cu migration.

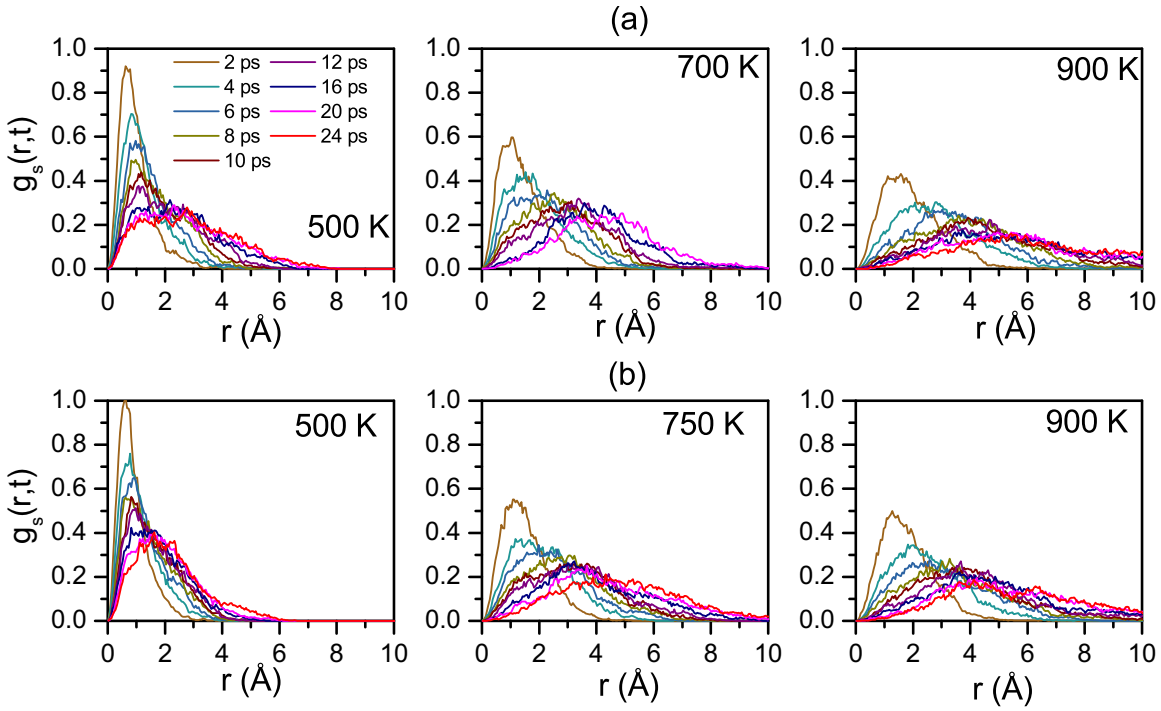

FIG. 5. The calculated Cu self–Van Hove correlation function $g_s(r,t)$ of (a) Cu_2Se superionic-cubic phase at 500, 700, and 900 K; (b) Cu_2S superionic phases at 500 K (hexagonal), 750, and 900 K (cubic).

anisotropic diffusion, even with the larger c/a (1.77) ratio. We have shown both results in Fig. S7 in the Supplemental Material [38].

We computed the self–Van Hove correlation function, $g_s(r,t)$ of Cu in Cu_2Se at 500, 700, and 900 K. The $g_s(r,t)$ computed at various time intervals from 2 to 26 ps are shown in Fig. 5. At all temperatures, $g_s(r,t)$ exhibits a peak around 1 Å in the first 2 ps, which gradually broadens with time; this implies that initially, Cu atoms are rattling within a cluster formed by 8c and 32f Wyckoff sites (the cluster diameter is ∼1 Å). Further, $g_s(r,t)$ at 500 K, shows a peak around 3 Å at later times, attributed to the Cu jumps from one cluster to another cluster along various possible channels (see Table I). This maximum centered around 3 Å is mainly contributed from tetrahedral to tetrahedral (T-T) Cu hopping along (100) and tetrahedral to octahedral (T-O) hopping along (111). Although broad it retains a peaklike structure in $g_s(r,t)$ at 500 K, suggesting that Cu^+ spends significant time near 4b/8c/32f sites and hence the Cu sublattice retains a discrete set of sites and hence Cu diffusion mainly occurs through discrete jumps and could be well described by jump-diffusion models. Interestingly, at 700 and 900 K, the first peak ∼1 Å swiftly decays, and $g_s(r,t)$ develop a very broad distribution of about 4 Å, inferring Cu spends less time in clusters around 8c sites and quickly hops to the next cluster. At higher temperatures, it is difficult to define the peak in $g_s(r,t)$, and hence it seems the Cu sublattice melts in Cu_2Se and behaves more like a liquid. The broad distribution of Cu around 4 Å is contributed from all possible Cu diffusion channels, namely, (T-T) Cu hopping along with all possible directions [(100), (111), and (111)], and (T-O) and O-O hopping along (111). The gradual shift of $g_s(r,t)$ distribution at higher distances at elevated temperatures indicates a more favorable hopping of Cu along (110) directions. Further, the $g_s(r,t)$ at 500 K takes ∼15–20 ps to span the distribution around 3 Å, while at 700 K within ∼10 ps, it spans around a 4 Å distance. This indicates that in Cu_2Se at 500 K, the diffusion of Cu is solidlike; however, at high temperatures of 700 and 900 K Cu diffusion can be described

TABLE I. (a) The intersite jump-length Cu-Cu in Cu_2Se and Cu_2S superionic-cubic phase, and (b) Cu_2S superionic hexagonal.

(a)

Hopping Cu Wyckoff sites	Hopping distance	
	Cu_2Se (cubic)	Cu_2S (cubic)
(T-T) Hopping in ⟨100⟩ directions (8c-8c)	2.92	2.88
(T-T) Hopping in ⟨110⟩ directions (8c-8c)	4.13	4.07
(T-O) Hopping in ⟨111⟩ directions (8c-4b)	2.53	2.49
(O-O) Hopping in ⟨110⟩ directions (4b-4b)	4.13	4.07

(b)

Hopping Cu Wyckoff sites	Hopping distance
	Cu_2S (hexagonal)
4f-6g	1.24
6g-6g	1.94
4f-4f	2.34
2b-6g	2.6

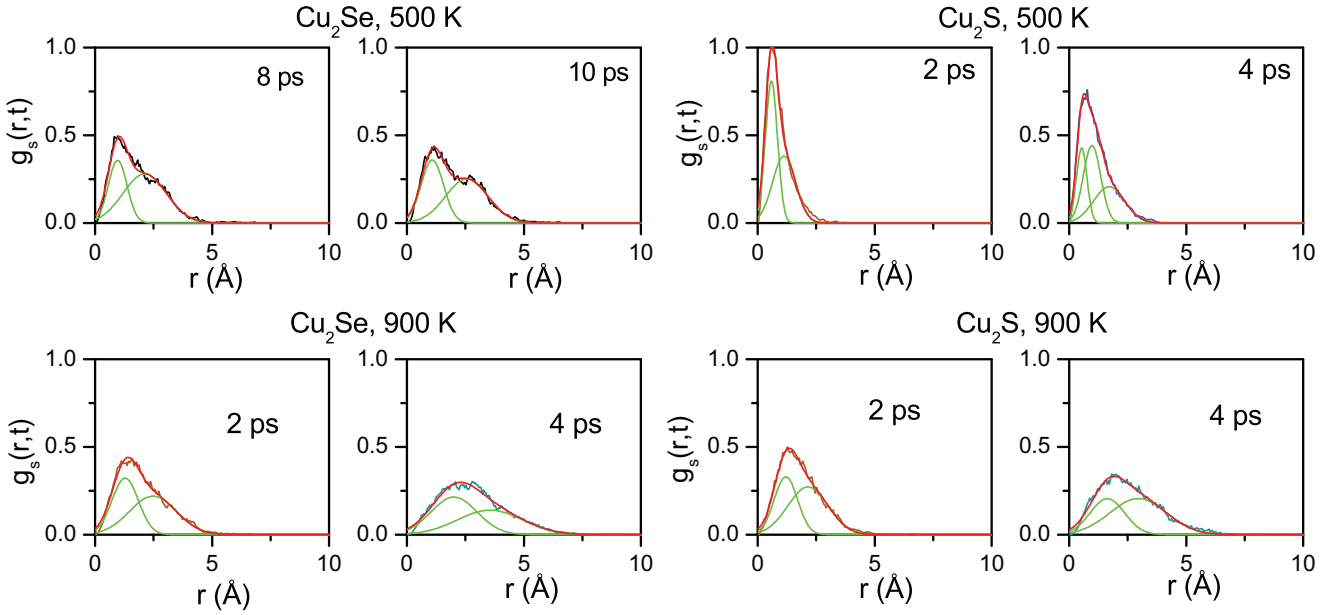

FIG. 6. The calculated self–van Hove correlation functions (black lines) at selected time intervals. The red lines show the least-squared fits comprising individual Lorentzian profiles (green lines); the results are given in Table II.

as liquidlike. Previous AIMD simulations [20,44] at 700 and 900 K also indicated liquidlike diffusion.

We have analyzed the $g_s(r,t)$ at selected time intervals (Fig. 6) by fitting the Lorentzian peaks at different intersite Cu-Cu distances to identify the jumplike and liquidlike diffusion behavior. For cubic Cu_2Se, at 500 K, the $g_s(r,t)$ shows the two distinct peaks at ∼1.2 and 2.92 Å corresponding to the Cu jumps within and between the clusters formed around 8*c* sites. The first peak (∼1.2 Å) originates from the intracluster jumps between 32*f* and 8*c* sites, while the second peak (∼2.92 Å) is attributed to intercluster jumps centered around 8*c* sites in Cu_2Se. We have fitted the two Lorentzians and estimated the FWHM of each peak. Here, the peak widths (1.1–1.3 Å) represent the size of the clusters. We obtained that the FWHM of each peak is less than the separation between the clusters (Table II). At 900 K, the peaks at 1.2 and 2.92 Å are not distinguishable, and the FWHM of intercluster jumps is ∼2.4 Å, which is significantly large, such that there is no clear separation of the two peaks. To summarize, at 500 K, we find a clear jumplike diffusion; at 900 K, the diffusion is not jumplike but liquidlike continuous diffusion.

The calculated self–Van Hove correlation function $g_s(r,t)$ in hexagonal and cubic phases of Cu_2S are shown in Fig. 5. At 500 K, in the hexagonal Cu_2S, $g_s(r,t)$ shows a sharp peak around 1 Å, which slowly decays, and distribution around 2.5 Å develops with time. The peak distribution around 2.5 Å is contributed from Cu hopping between various Cu sites (6*g*-6*g*, 4*f*-4*f*, and 2*b*-6*g* sites). At 700 K, the peak in $g_s(r,t)$ at ∼1 Å becomes broad and swiftly decays, and very broad distribution of about 3 Å is evolved. In the cubic Cu_2S, the first peak at ∼1.3 Å originates from the intracluster jumps between 192*l* and 8*c* sites. Interestingly, in the cubic phase of Cu_2S, $g_s(r,t)$ at 750 and 900 K shows a much faster decay of the 1 Å peak and shows a broad distribution around 4 Å, similar to the case of cubic Cu_2Se.

The analysis of the Van Hove self-correlation function shows (Fig. 6 and Table II) that at 500 K in hexagonal Cu_2S, the diffusion occurs between closely spaced sites. The first

TABLE II. The estimated Lorentzian widths of $g_s(r,t)$ at selected time intervals in Cu_2Se and Cu_2S at 500 and 900 K (from the fits shown in Fig. 6). The first peak (∼1.2 Å) in cubic Cu_2Se originates from the intracluster jumps between 32*f* and 8*c* sites. In the hexagonal phase of Cu_2S, the peak at ∼0.6 Å occurs due to the phonon vibrations around the original position. In the cubic Cu_2S, the first peak at ∼1.27 Å originates from the intracluster jumps between 192*l* and 8*c* sites. Other peak position correspond to neighboring crystalline sites.

Cu_2Se (cubic phase)				
T (K)	500 K		900 K	
T (ps)	8	10	2	4
d (Å)	FWHM	FWHM	FWHM	FWHM
1.2	1.44 ± 0.02	1.30 ± 0.02	1.35 ± 0.04	1.22 ± 0.07
2.92	1.08 ± 0.06	1.34 ± 0.04	1.87 ± 0.09	2.43 ± 0.04

Cu_2S (hexagonal phase)		
T (K)	500 K	
t (ps)	2	4
d (Å)	FWHM	FWHM
0.63	0.61 ± 0.01	0.60 ± 0.01
1.24	0.76 ± 0.03	0.91 ± 0.05
1.94		0.81 ± 0.11

Cu_2S 900 K (cubic phase)		
T (K)	900 K	
t (ps)	2	4
d (Å)	FWHM	FWHM
1.27	1.33 ± 0.03	1.34 ± 0.05
2.88	1.52 ± 0.1	2.17 ± 0.05

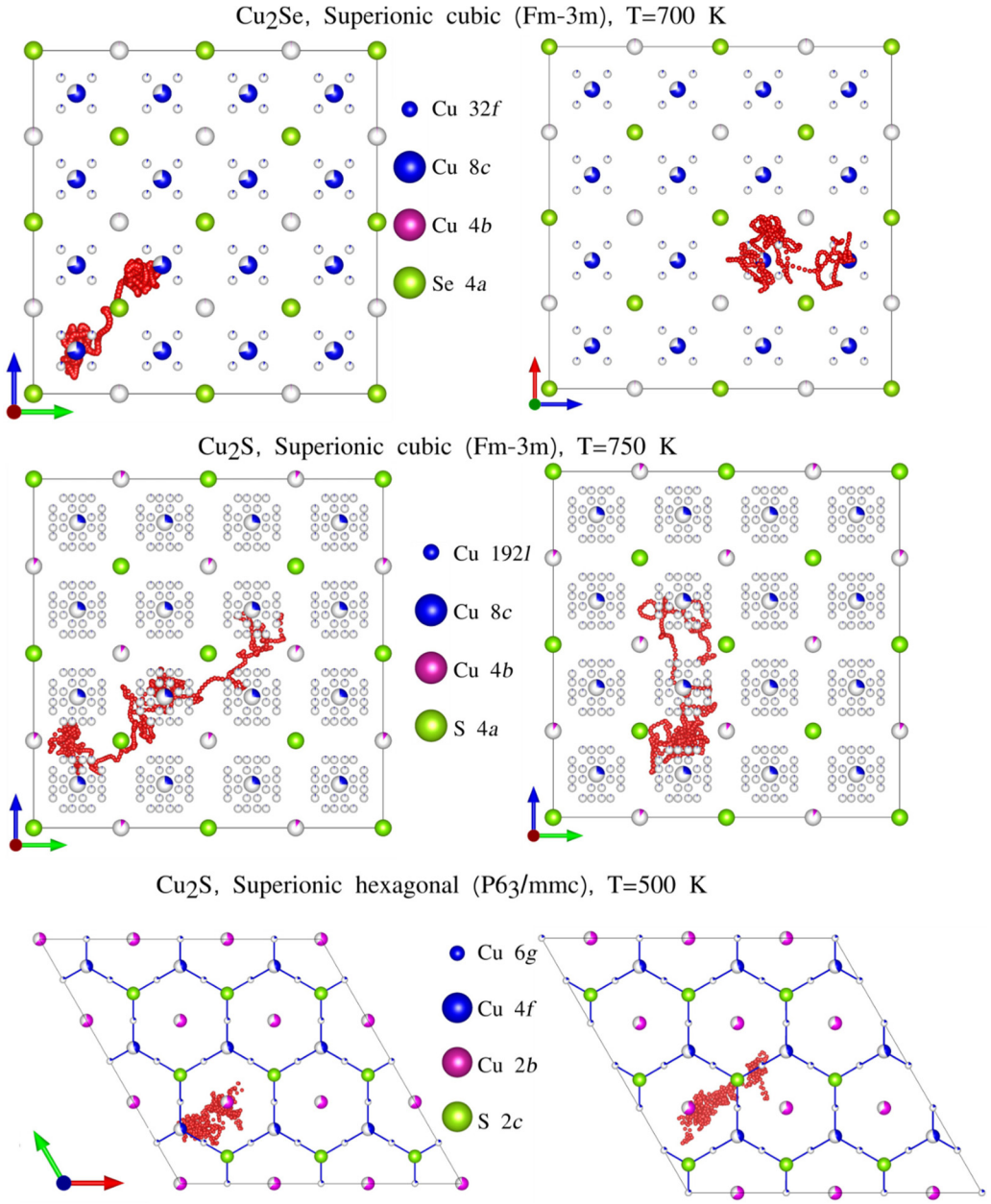

FIG. 7. The calculated Cu trajectories of a few representative Cu's in superionic phases of Cu_2X (X = S, Se). The Cu trajectories are shown by the red dotted line, while the average Cu and X positions are shown by spheres. Details of the average Cu and X sites are shown in the legends. Cu trajectory in cubic Cu_2Se (top panel) and cubic Cu_2S (middle panel) shows hops between tetrahedral sites (8c) via an octahedral site (4b), and also direct jumps. Cu trajectory in hexagonal Cu_2S (bottom panel) shows hops from 2b to 4f sites. In addition, all the trajectories show localized diffusion around the respective sites.

peak at ∼0.6 Å in the hexagonal phase occurs due to the phonon vibrations around the original position. The positions of other nearest neighbor available jumps are summarized in Tables I and II. The FWHM values (Table II) of Van Hove peaks in the hexagonal phase are comparable to the separation between the neighboring sites. Thus, the diffusion appears to be liquidlike as the atomic distribution is spread out significantly away from the crystal sites. At 900 K, in cubic Cu_2S, the larger FWHM values clearly indicate a liquidlike continuous diffusion.

To visualize the diffusion process, we plotted the trajectories of a few Cu atoms in the superionic-cubic phase in Cu_2Se at 700 K (Fig. 7). We can see that, at 700 K, Cu hops from one tetrahedral (8c) to another tetrahedral site (8c) either via an octahedral site (4b) or a direct jump, consistent with previous reports [23,44]. Further, by observing the individual Cu trajectories, we could see that Cu ions rattle around 8c (i.e., hopping among 32f sites) for extended times before making a jump to the next tetrahedral site. The hopping among 32f sites is much faster and leads to a localized component in the Cu diffusion, while the tetrahedral to tetrahedral Cu hops, which contribute to long-range diffusion, are slower**.** To identify the Cu hopping pathways, we have computed the probability density at 700 K for Cu atoms in the (0 0 $\frac{1}{2}$) and

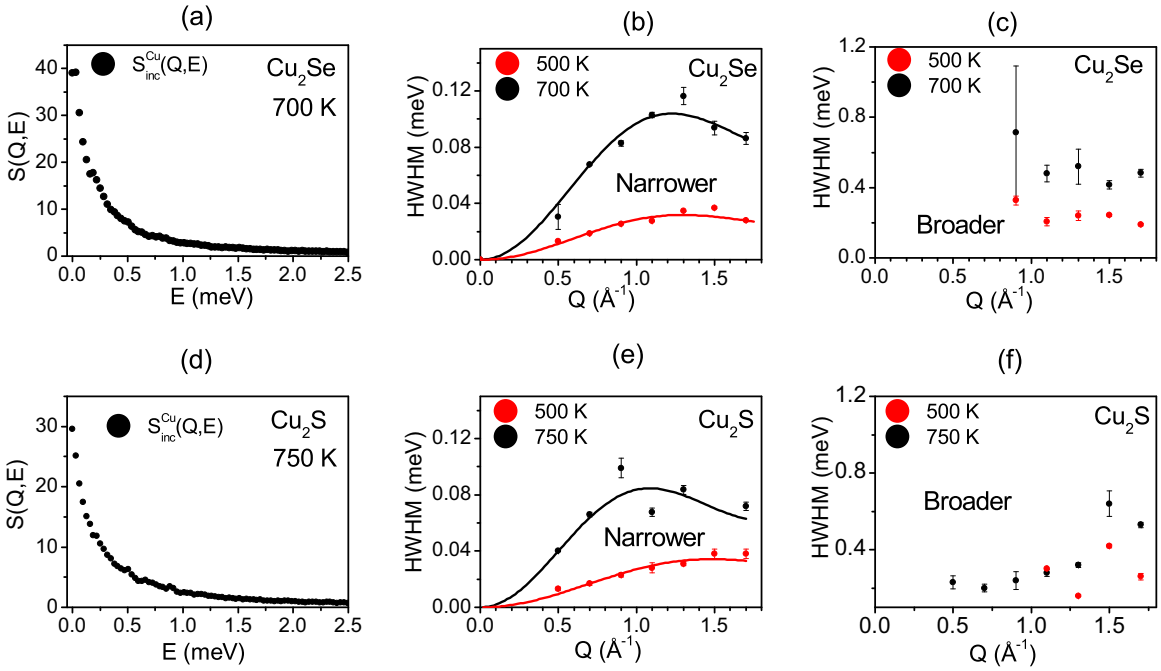

FIG. 8. (a), (d) The calculated incoherent $[S^{Cu}_{inc}(Q, E)]$ dynamical structure factors in superionic cubic phases of Cu_2X (X = S, Se). (b), (e) The estimated Q dependence of the narrower Lorentzian HWHM from the incoherent $S^{Cu}_{inc}(Q, E)$ in superionic phases of Cu_2Se (Cu_2S) at T = 500 K (500 K) and 700 K (750 K) is shown by the black and red markers, respectively. The solid lines in (b), (d) are the CE model fit to respective HWHM and (c), (f) the estimated Q dependence of the broader Lorentzian HWHM from incoherent $S^{Cu}_{inc}(Q, E)$ in Cu_2Se and Cu_2S.

(0 0 $\frac{1}{4}$) planes, which contain the octahedral and tetrahedral Cu sites, respectively (Fig. S6 in the Supplemental Material [38]). From the probability density plots, it appears that the main hopping channels are Cu hopping from a tetrahedral site to another site via octahedral sites.

In the superionic hexagonal phase of Cu_2S, we found that Cu diffusion is nearly isotropic (Fig. S7 in the Supplemental Material [38]), which is in contrast with previously reported [37] AIMD simulations. In the hexagonal phase, to visualize the nature of diffusion, we also plotted the trajectories of a few Cu atoms at 500 K (Fig. 7). Further, by observing the individual Cu trajectories, we can see that Cu also rattles around the 4*g* and 6*b* sites (localized diffusion) followed by a jump to 2*b* sites (long-range diffusion). The superionic-cubic phase of Cu_2S exhibits similar attributes of Cu diffusion as observed in superionic cubic Cu_2Se. From the trajectory analysis at 750 K shown in Fig. 7, we found that there are two types of jump present in the system; the first is dwelling between 192*l* and 8*c* sites that contributes to localized diffusion, while the second kind of jump (i.e., tetrahedral to tetrahedral jump) contributes to long-range diffusion.

C. Dynamic structure factor $S(Q, E)$

Several QENS experiments have been reported [21,23,44] that addressed the Cu diffusion behavior in the superionic-cubic phase of Cu_2Se. The results have been analyzed using the CE jump-diffusion model. The first QENS measurements on the superionic phase of Cu_2Se were performed by Danilkin *et al.* [23]. The authors used a single Lorentzian in their analysis, equivalent to considering only a single kind of Cu hopping, and estimated $D \sim 6.1 \times 10^{-5}$ cm^2 s^{-1}. Another QENS investigation by Voneshen *et al.* [21] showed two different jump timescales for the localized and long-range diffusion, respectively, and estimated a $D \sim 5$–35×10^{-7} cm^2 s^{-1} over 500–900 K. Another recent QENS study at 675 K by Islam *et al.* [44] estimated a $D \sim 3.4 \times 10^{-5}$ cm^2 s^{-1}.

In all the above QENS studies, the analysis was based on the CE model assuming incoherent scattering due to independent jumps. Here, we have simulated the incoherent dynamical structure factor of Cu in Cu_2X (X = S, Se), $S^{Cu}_{inc}(Q, E)$, at different temperatures ranging from 500 to 900 K, to investigate the jump-length distribution and associated timescale and diffusion constants.

Cu_2Se. Our calculated incoherent dynamical structure factor for Cu in superionic Cu_2Se at 700 K is shown in Fig. 8. To estimate D, we use $S^{Cu}_{inc}(Q, E)$, which represents the random/stochastic diffusion process, and justifies the use of the CE model. We have first analyzed the calculated $S^{Cu}_{inc}(Q, E)$ with a single Lorentzian and noticed a significant discrepancy between the calculated $S^{Cu}_{inc}(Q, E)$ and the fit (Fig. S8(a) in the Supplemental Material [38]). Interestingly, two Lorentzians excellently describe the calculated $S^{Cu}_{inc}(Q, E)$, suggesting two kinds of diffusive dynamics present in the system (Fig. S8(b) in the Supplemental Material [38]). The widths of the two Lorentzians differ by an order of magnitude, which implies the two dynamics occur on very different timescales. The fast diffusion dynamics is reflected in the Lorentzian with a larger width, while the slower diffusion gives the smaller Lorentzian width. The Q dependence of the HWHM of the Lorentzian peak provides direct information about diffusion characteristics. The estimated Q dependences of the HWHM

TABLE III. The calculated diffusion coefficient D, jump length (d), and residence time (τ) of Cu in different phases of Cu_2X (X = S, Se) from fits using CE model.

	d (Å)	τ (ps)	D (10^{-6} cm^2/s)
Cu_2Se cubic (700 K) from incoherent $S(Q, E)$ from simulation	3.7 ± 0.1	7.7 ± 0.2	29 ± 2
Cu_2Se cubic (500 K) from incoherent $S(Q, E)$ from simulation	3.5 ± 0.2	25 ± 2	8 ± 2
Cu_2Se cubic (Islam *et al.* [44]) (675 K) from total $S(Q, E)$ from QENS	2.8 ± 0.2	3.7 ± 0.12	34
Cu_2S hexagonal (500 K) from incoherent $S(Q, E)$ from simulation	3.0 ± 0.2	23.4 ± 1.7	6.4 ± 1.3
Cu_2S cubic (750 K) from incoherent $S(Q, E)$ from simulation	4.1 ± 0.2	9.5 ± 0.6	30 ± 5

of the Lorentzian for superionic-cubic Cu_2Se at 500 and 700 K are shown in Figs. 8(b) and 8(c). We find that the HWHM of the slower dynamics Lorentzian, Γ_1, shows a Q^2 behavior at low Q. This indicates the presence of long-range diffusion. In contrast, the higher value of HWHM from the second Lorentzian, Γ_2, remains nearly independent of Q, signifying the presence of fast localized diffusion, attributed to hopping among $32f$ sites around the tetrahedral $8c$ sites.

Our estimated Q-dependent Γ_1 from $S_{\rm inc}(Q, E)$ for the cubic phase of Cu_2Se at 700 K is underestimated by about a factor of 2 compared to the values reported from the QENS measurement at 700 K by Islam *et al.* [44]. The Q-dependent Γ_1 at 500 and 700 K is analyzed with the CE model. The fitted residence time τ, jump length d, and estimated diffusion constant D are summarized in Table III. Our estimated D from the CE model at 700 K is in fair agreement with the QENS estimated $D \sim 3 \times 10^{-5}$ cm^2/s by Islam *et al.* [44].

Cu_2S. In Fig. 8(d), we show the computed $S^{\rm Cu}_{\rm inc}(Q, E)$ of superionic-cubic Cu_2S at 750 K. Here also, two Lorentzians are required to describe the $S^{\rm Cu}_{\rm inc}(Q, E)$ in both superionic phases, i.e., cubic and hexagonal (Fig. S8 in the Supplemental Material [38]), corresponding to the faster and slower dynamics, respectively. Further, we have used Q dependence of narrower HWHM from $S^{\rm Cu}_{\rm inc}(Q, E)$ to estimate D via a CE jump-diffusion model [Fig. 8(e)]. The fitted parameters and estimated D for superionic-hexagonal and cubic phases at 500 and 750 K, are summarized in Table III. The estimated D from the CE model for the hexagonal phase at 500 K and cubic phase at 750 K is $\sim 6.4 \times 10^{-6}$ cm^2 s^{-1} and $\sim 3.0 \times 10^{-5}$ cm^2 s^{-1}, respectively. The presence of the fast localized diffusion, attributed to hopping among $192l$ sites around the tetrahedral $8c$ sites, is similar to Cu_2Se.

D. Diffusion coefficient using various approaches

The MSD plots of Fig. 4 are used to calculate the temperature-dependent diffusion coefficients. Further, we have calculated the relative standard deviation (RSD) of the estimated diffusion constant (Table IV) using an empirical relation as described in Ref. [62]. RSD of diffusion constant depends on the number of total jump events during the simulation time ($N_{\rm eff}$) as given by

$$\text{RSD} = 3.43/\sqrt{N_{\rm eff}} + 0.04, \tag{9}$$

$$N_{\rm eff} = \text{TMSD}/d^2_{\rm jump}, \tag{10}$$

where TMSD is total mean-squared displacement defined as the sum of all Cu MSD in the simulation cell, and $d_{\rm jump}$ is the mean jump length of the Cu atom. In the case of the cubic and the hexagonal phases, the mean jump length is taken as $\sim$3.2 Å. The analysis was performed on a 30 ps trajectory length.

Further, we used the MSD estimated D to estimate the energy barrier E_a for Cu migration in Cu_2X (X = S/Se) using

TABLE IV. The calculated diffusion coefficient D of Cu in different phases of Cu_2X (X = S, Se) from suites of numerical techniques. The estimated relative standard deviation (RSD) of diffusion coefficient (D) from MSD as described in Ref. [62]. The analysis was performed on 30 ps trajectory length. The results from the CE jump-diffusion model differ significantly from that from MSD and VACF, which indicates that the CE model is oversimplified and does not adequately describe the diffusion.

T(K)	D from MSD (10^{-6} cm^2/s)	D from VACF (10^{-6} cm^2/s)	D from CE model fitting (10^{-6} cm^2/s)	PRB [20] (10^{-6} cm^2/s)		Relative standard deviation (RSD) of D (in %) $3.4/\sqrt{N_{\rm eff}} + 0.04$
				MSD	VACF	
		Cu_2Se (superionic cubic)				
500	5.4	4.4	11.1 ± 0.2			41
700	21	17	29 ± 2			30
900	36	36		34	34	21
		Cu_2S (superionic hexagonal)				
500	5.2	4.3	6.4 ± 1.3			28
700	16	13	29 ± 4			23
		Cu_2S (superionic cubic)				
750	17	22	30 ± 5			42
900	29	30		33	35	24

the Arrhenius relation as given by [63]

$$\ln[D(T)] = \ln(D_0) - E_a/k_B T. \quad (11)$$

D_0 is the prefactor factor; k_B is the Boltzmann constant. The estimated value of the activation energy barrier of Cu atoms is 0.17, 0.16, and 0.18 eV for Cu_2Se (superionic cubic), Cu_2S (superionic hexagonal), and Cu_2S (superionic cubic), respectively, as shown in Fig. 4. These values are in fair agreement with reported activation energy barrier ($E_a \sim 0.15$ eV for the cubic phase of Cu_2Se and $E_a \sim 0.19$ eV for the hexagonal phase of Cu_2S) from electronic impedance spectroscopy [64,65].

In Table IV, we summarized the calculated D from different numerical techniques and also show the relative error from these methods. We further estimated the ionic conductivity using the Nernst-Einstein relation. We found that the Cu ionic conductivity at 700 K in Cu_2Se from computed D from different schemes lies in the range of 1.5–3.0 Ω^{-1} cm^{-1} which is in excellent agreement with the reported conductivity at 673 K [64]. This further confirms that Cu diffusion is well captured in our simulations.

V. CONCLUSIONS

We have presented INS measurements on $Cu_{1.95}Se$, and lattice dynamics, and AIMD simulation in Cu_2X (X = S, Se) to investigate Cu diffusion. We are able to identify the nature of diffusion at low and moderate temperatures, a solidlike diffusion comprising (a) the localized jumps among a small cluster of sites around the tetrahedral site, and (b) long-range diffusion involving jumps to the first and the second nearest neighbor sites. At high temperatures of ∼900 K, the diffusion is liquidlike, which is not restricted to jumps among definite crystal sites. We have also calculated the diffusion coefficients using different approaches, namely, the mean-squared displacements, velocity autocorrelation, and the jump-diffusion model of the dynamical structure factor. While the first two approaches produce consistent results, we find that the jump-diffusion model assuming jumps over a fixed distance in the present case of Cu_2X is an oversimplification and does not produce consistent results of the diffusion coefficient. However, the range of the magnitude of the diffusion coefficient and the derived ionic conductivity are in fair agreement with the reported experimental values.

ACKNOWLEDGMENTS

The use of the ANUPAM supercomputing facility at BARC is acknowledged. S.L.C. acknowledges the financial support of the Indian National Science Academy for the INSA Senior Scientist position.

[1] A. J. E. Rettie, J. Ding, X. Zhou, M. J. Johnson, C. D. Malliakas, N. C. Osti, D. Y. Chung, R. Osborn, O. Delaire, S. Rosenkranz, M. G. Kanatzidis *et al.*, Nat. Mater. **20**, 1683 (2021).
[2] S. Liu, W. Xia, K. Huang, D. Pei, T. Deng, A. J. Liang, J. Jiang, H. F. Yang, J. Zhang, H. J. Zheng *et al.*, Phys. Rev. B **103**, 115127 (2021).
[3] A. Würger, Phys. Rev. Lett. **126**, 068001 (2021).
[4] M. Ochi, H. Mori, D. Kato, H. Usui, and K. Kuroki, Phys. Rev. Materials **2**, 085401 (2018).
[5] J. Min, A. K. Sagotra, and C. Cazorla, Phys. Rev. Materials **4**, 015403 (2020).
[6] D. Byeon *et al.*, Nat. Commun. **10**, 72 (2019).
[7] D.-l. Shi, Z.-m. Geng, L. Shi, Y. Li, and K.-h. Lam, J. Mater. Chem. C **8**, 10221 (2020).
[8] H. Liu *et al.*, Nat. Mater. **11**, 422 (2012).
[9] S. L. White, P. Banerjee, and P. K. Jain, Nat. Commun. **8**, 14514 (2017).
[10] H. Kim, S. Ballikaya, H. Chi, J.-P. Ahn, K. Ahn, C. Uher, and M. Kaviany, Acta Mater. **86**, 247 (2015).
[11] Y. He, T. Day, T. Zhang, H. Liu, X. Shi, L. Chen, and G. J. Snyder, Adv. Mater. **26**, 3974 (2014).
[12] B. Gahtori, S. Bathula, K. Tyagi, M. Jayasimhadri, A. K. Srivastava, S. Singh, R. C. Budhani, and A. Dhar, Nano Energy **13**, 36 (2015).
[13] S. Kashida, W. Shimosaka, M. Mori, and D. Yoshimura, J. Phys. Chem. Solids **64**, 2357 (2003).
[14] R. Marshall and S. Mitra, J. Appl. Phys. **36**, 3882 (1965).
[15] L. Liu, C. Liu, W. Fu, L. Deng, and H. Zhong, ChemPhysChem **17**, 771 (2016).
[16] C. Pan, S. Niu, Y. Ding, L. Dong, R. Yu, Y. Liu, G. Zhu, and Z. L. Wang, Nano Lett. **12**, 3302 (2012).
[17] H. Komaki, M. Iioka, A. Yamada, S. Furue, S. Ishizuka, K. Matsubara, H. Shibata, and S. Niki, Jpn. J. Appl. Phys. **51**, 10NC04 (2012).
[18] D. Chakrabarti and D. Laughlin, Bull. Alloy Phase Diagrams **2**, 305 (1981).
[19] D. Chakrabarti and D. Laughlin, Bull. Alloy Phase Diagrams **4**, 254 (1983).
[20] K. Zhuo, J. Wang, J. Gao, U. Landman, and M.-Y. Chou, Phys. Rev. B **102**, 064201 (2020).
[21] D. J. Voneshen, H. C. Walker, K. Refson, and J. P. Goff, Phys. Rev. Lett. **118**, 145901 (2017).
[22] T. Takahashi, O. Yamamoto, F. Matsuyama, and Y. Noda, J. Solid State Chem. **16**, 35 (1976).
[23] S. Danilkin, M. Avdeev, T. Sakuma, R. Macquart, C. Ling, M. Rusina, and Z. Izaola, Ionics **17**, 75 (2011).
[24] L. Gulay, M. Daszkiewicz, O. Strok, and A. Pietraszko, Chem. Met. Alloys **4**, 200 (2011).
[25] M. A. Korzhuev, Phys. Solid State **40**, 217 (1998).
[26] R. Yakshibaev, V. Konev, and M. K. Balapanov, Fiz. Tverd. Tela (Leningrad) **26**, 3641 (1984) [Sov. Phys. Solid State **26**, 2189 (1984)].
[27] N. Kh. Abrikosov, V. F. Bankina, M. A. Korzhuev, G. K. Demenskii, and O. A. Teplov, Fiz. Tverd. Tela **25**, 2911 (1983).
[28] A. Skomorokhov, D. Trots, M. Knapp, N. Bickulova, and H. Fuess, J. Alloys Compd. **421**, 64 (2006).
[29] E. Eikeland, A. B. Blichfeld, K. A. Borup, K. Zhao, J. Overgaard, X. Shi, L. Chen, and B. B. Iversen, IUCrJ **4**, 476 (2017).
[30] S. A. Danilkin, A. N. Skomorokhov, A. Hoser, H. Fuess, V. Rajevac, and N. N. Bickulova, J. Alloys Compd. **361**, 57 (2003).
[31] M. J. Buerger and B. J. Wuensch, Science **141**, 276 (1963).
[32] H. T. Evans, Nat. Phys. Sci. **232**, 69 (1971).

[33] H. T. Evans, Science **203**, 356 (1979).
[34] D. Zimmer, J. Ruiz-Fuertes, L. Bayarjargal, E. Haussühl, B. Winkler, J. Zhang, C. Q. Jin, V. Milman, E. Alig, and L. Fink *et al.*, Phys. Rev. B **96**, 054108 (2017).
[35] G. Will, E. Hinze, and A. R. M. Abdelrahman, Eur. J. Mineral. **14**, 591 (2002).
[36] J. Wang, K. Zhuo, J. Gao, U. Landman, and M.-Y. Chou, Phys. Rev. Materials **5**, 073603 (2021).
[37] L.-W. Wang, Phys. Rev. Lett. **108**, 085703 (2012).
[38] See Supplemental Material at http://link.aps.org/supplemental/10.1103/PhysRevMaterials.6.055403 for details about the characterization of the sample and the results of calculated pair distribution functions of various pairs of atoms, and time-dependent mean-squared displacements in various phases of Cu2X (X = Se, S).
[39] J. P. Boilot, P. Colomban, R. Collongues, G. Collin, and R. Comès, Phys. Rev. Lett. **42**, 785 (1979).
[40] J. X. Zheng-Johansson, K. Sköld, and J.-E. Jørgensen, Solid State Ionics **70**, 522 (1994).
[41] J. Johansson, K. Sköld, and J. Jørgensen, Solid State Ionics **50**, 247 (1992).
[42] T. W. D. Farley, W. Hayes, S. Hull, M. T. Hutchings, M. Alba, and M. Vrtis, Physica B **156–157**, 99 (1989).
[43] M. Gupta, B. Singh, P. Goel, R. Mittal, S. Rols, and S. L. Chaplot, Phys. Rev. B **99**, 224304 (2019).
[44] S. M. K. Nazrul Islam *et al.*, Acta Mater. **215**, 117026 (2021).
[45] J. M. Carpenter and D. L. Price, Phys. Rev. Lett. **54**, 441 (1985).
[46] D. L. Price and K. Skold, in *Methods in Experimental Physics*, edited by K. Sköld and D. L. Price (Academic Press, New York, 1986), p. 1.
[47] S. W. Lovesey, *Theory of Neutron Scattering from Condensed Matter* (Clarendon Press, Oxford, UK, 1984).
[48] G. Kresse and J. Furthmüller, Phys. Rev. B **54**, 11169 (1996).
[49] J. Hafner, J. Comput. Chem. **29**, 2044 (2008).
[50] J. P. Perdew, K. Burke, and M. Ernzerhof, Phys. Rev. Lett. **77**, 3865 (1996).
[51] G. Kresse and D. Joubert, Phys. Rev. B **59**, 1758 (1999).
[52] A. Togo and I. Tanaka, Scr. Mater. **108**, 1 (2015).
[53] H. J. Monkhorst and J. D. Pack, Phys. Rev. B **13**, 5188 (1976).
[54] J.-P. Hansen and I. R. McDonald, *Theory of Simple Liquids: With Applications to Soft Matter* (Academic Press, New York, 2013).
[55] M. P. Allen and D. J. Tildesley, *Computer Simulation of Liquids*, 2nd ed. (Oxford University Press, Oxford, 2017).
[56] A. K. Sagotra, D. Chu, and C. Cazorla, Phys. Rev. Materials **3**, 035405 (2019).
[57] P. A. Ferrari, S. Goldstein, and J. L. Lebowitz, in *Statistical Physics and Dynamical Systems* (Springer, Berlin, 1985), p. 405.
[58] M. Bée, *Quasielastic Neutron Scattering* (Adam Hilger, Bristol, UK, 1988).
[59] P. L. Hall and D. Ross, Mol. Phys. **42**, 673 (1981).
[60] C. Chudley and R. Elliott, Proc. Phys. Soc. **77**, 353 (1961).
[61] L. Van Hove, Phys. Rev. **95**, 1374 (1954).
[62] X. He, Y. Zhu, A. Epstein, and Y. Mo, npj Comput. Mater. **4**, 18 (2018).
[63] A. K. Galwey and M. Brown, Proc. R. Soc. London, Ser. A: Mathematical and Physical Sciences **450**, 501 (1995).
[64] M. K. Balapanov, A. Nadejzdina, R. Yakshibayev, D. Lukmanov, and R. J. Gabitova, Ionics **5**, 20 (1999).
[65] M. K. Balapanov, I. Gafurov, U. K. Mukhamed'Yanov, R. Yakshibaev, and R. K. Ishembetov, Phys. Status Solidi B **241**, 114 (2004).